

# Modelling the circle of Willis to assess the effects of anatomical variations and occlusions on cerebral flows

J. Alastruey<sup>a,b</sup>, K.H. Parker<sup>b</sup>, J. Peiró<sup>a</sup>, S.M. Byrd<sup>c</sup>, S.J. Sherwin<sup>a,\*</sup>

<sup>a</sup>Department of Aeronautics, South Kensington Campus, Imperial College London, SW7 2AZ, UK

<sup>b</sup>Department of Bioengineering, South Kensington Campus, Imperial College London, SW7 2AZ, UK

<sup>c</sup>NHLI, International Centre for Circulatory Health, Imperial College London, W2 1LA, UK

Accepted 28 July 2006

## Abstract

Blood flow in the circle of Willis (CoW) is modelled using the 1-D equations of pressure and flow wave propagation in compliant vessels. The model starts at the left ventricle and includes the largest arteries that supply the CoW. Based on published physiological data, it is able to capture the main features of pulse wave propagation along the aorta, at the brachiocephalic bifurcation and throughout the cerebral arteries. The collateral ability of the complete CoW and its most frequent anatomical variations is studied in normal conditions and after occlusion of a carotid or vertebral artery (VA). Our results suggest that the system does not require collateral pathways through the communicating arteries to adequately perfuse the brain of normal subjects. The communicating arteries become important in cases of missing or occluded vessels, the anterior communicating artery (ACoA) being a more critical collateral pathway than the posterior communicating arteries (PCoAs) if an internal carotid artery (ICA) is occluded. Occlusions of the VAs proved to be far less critical than occlusions of the ICAs. The worst scenario in terms of reduction in the mean cerebral outflows is a CoW without the first segment of an anterior cerebral artery combined with an occlusion of the contralateral ICA. Furthermore, in patients without any severe occlusion of a carotid or VA, the direction of flow measured at the communicating arteries corresponds to the side of the CoW with an absent or occluded artery. Finally, we study the effect of partial occlusions of the communicating arteries on the cerebral flows, which again confirms that the ACoA is a more important collateral pathway than the PCoAs if an ICA is occluded.

© 2006 Elsevier Ltd. All rights reserved.

**Keywords:** Circle of Willis; Anatomical variations; Collateral flow; One-dimensional modelling; Pulse wave propagation

## 1. Introduction

The brain critically depends on the cerebral circulation since it has a high metabolic rate and is very sensitive to ischemia (insufficient blood supply). Sufficient blood supply to the brain is maintained by a network of collateral vessels and a precise system of autoregulation by vasodilatation and vasoconstriction. Blood is delivered to the brain through the two internal carotid arteries (ICAs) and the two vertebral arteries (VAs) (see Fig. 1, left). Each ICA bifurcates to form a middle cerebral artery (MCA) and an anterior cerebral artery (ACA) to perfuse the temporal, parietal and frontal regions of the brain (anterior circula-

tion). The two VAs anastomose into the basilar artery, which divides into the right and left posterior cerebral arteries (PCAs) to deliver blood to the regions of the brain stem (posterior circulation). The anterior and the posterior circulations are interconnected by the anterior and posterior communicating arteries (ACoA and PCoAs). The resulting ring-like arterial structure, called the circle of Willis (CoW), is the main collateral pathway in the cerebral circulation. It provides collateral blood supply to the efferent (outflow) arteries in case of missing or occluded vessels.

Unfortunately, many anatomical variations of the haemodynamically complete and well-balanced CoW shown in Fig. 1 (left) are commonly observed. Based on more than 50 radiological and anatomical studies, Lippert and Pabst (1985) found that about 50% of the population

\*Corresponding author. Tel.: +44 20 7594 5052; fax: +44 20 7584 8120.  
E-mail address: s.sherwin@imperial.ac.uk (S.J. Sherwin).

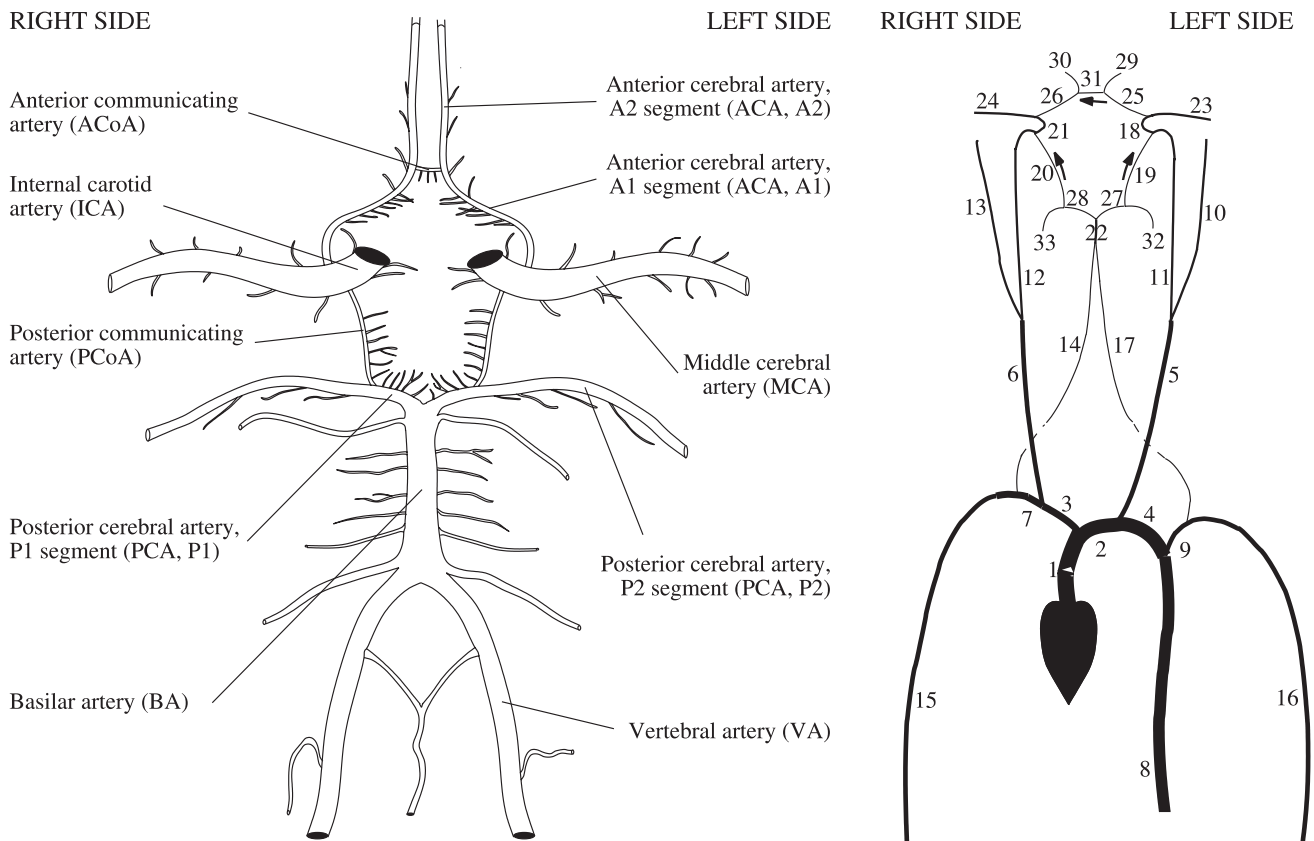


Fig. 1. Schematic representation of the circle of Willis (left) and of the arterial network simulated (right), which includes the aorta, brachial, carotid, vertebral and the main cerebral arteries. Numbers refer to names in Table 1 and arrows in the communicating arteries indicate the positive flow directions.

has a CoW with at least one artery absent or hypoplastic (very small or incompletely developed). These anatomical variations reduce the collateral availability and increase the risk of stroke and transient ischemic attack (TIA) in patients with severe stenosis in an ICA (Henderson et al., 2000). Knowledge of the compensatory capacity of the CoW is important for neurosurgeons, vascular surgeons and interventional radiologists when a procedure in the intracranial or extracranial cerebral arteries is to be attempted (Hoksbergen et al., 2003). Such procedures include carotid endarterectomy (surgical incision in the carotid artery to remove plaque in patients with a severe carotid stenosis), angioplasty (balloon expansion of an artery) and stenting (introduction of a mesh to keep the lumen open after angioplasty) (Henderson et al., 2000; Cebal et al., 2003).

Several mathematical studies have been carried out to investigate the capability of the CoW to reduce the effects of haemodynamic pathological alterations. According to Hillen et al. (1986) and based on a non-linear, 1-D model of a complete and well-balanced CoW, blood flows in the afferent (inflow) vessels and in the segments of the CoW of healthy subjects are strongly influenced by their own resistances, whereas flow in the efferent vessels is dominated by the peripheral resistances. With a similar model of the CoW, Cassot et al. (1995) claimed that small changes in the diameter of the ACoA (within the range of 0.4–1.6 mm)

have a strong influence on regulating cerebral haemodynamics in case of ICA stenosis. Viedma et al. (1997) investigated different combinations of the diameters of the communicating arteries that can lead to insufficient cerebral perfusion in case of an occlusion of an ICA. Moorhead et al. (2004) used a linear, 1-D model with time-varying resistances in the efferent vessels to account for vasodilatation and vasoconstriction. They showed that the omission of a single circulus vessel can be compensated for by the CoW and autoregulation to maintain the required efferent flow rates in case of an occlusion of an ICA. Although their model neglects flow pulsatility, it offers the possibility of analytical solutions (Hillen et al., 1988; Cassot et al., 2000). The problem has also been approached with a non-linear, 2-D model with time-varying resistances, but with rigid arterial walls (Ferrandez et al., 2002; David et al., 2003). Ferrandez et al. (2002) found that the worst configuration of the CoW when an ICA is partially occluded is that of a missing ipsilateral A1 segment of the ACA. David et al. (2003) suggested that the PCoA and other small arteries of the CoW, which are often non-visible by non-invasive magnetic-resonance (MR) techniques, can be better visualised by performing the scan at the specific point in time when the flux is maximum according to the simulation. They also pointed out that any simulation will be improved if it can take into account the correct time delay between the inlet flow waves at the

ICAs and VAs. Several 3-D models have been used to simulate the injection of a contrast agent and to study wall-shear stress distributions (Cebal et al., 2003), to investigate the role played by haemodynamics in the formation, development and rupture of cerebral aneurysms (Oshima, 2004), and to study autoregulation (Moore et al. 2005,2006).

In this study, we apply a previously published non-linear, 1-D algorithm (Sherwin et al., 2003b) to simulate blood flow wave propagation in an elastic model of the cerebral arteries that includes the aorta, the subclavian arteries (SCAs), the brachial arteries, the common carotid arteries (CCAs), the external carotid arteries (ECAs) and the VAs (Fig. 1, right). In this model, the time delay between the inflow waves at the ICAs and VAs is implicitly determined by the pulse wave speeds of the vessels supplying them from the ascending aorta. Only an inflow boundary condition at the ascending aorta is required. Although 3-D models consider a better definition of the geometry and they might account for the deformation of the arterial wall, they are computationally too expensive to simulate pulse wave propagation in our model of the CoW. Because of the large wavelength of the arterial pulse compared to the arterial diameters, 1-D modelling permits an efficient and fast simulation of pulse wave propagation. The accuracy of our 1-D model has been successfully validated in Alastruey (2006) against a well-defined hydrodynamic 1:1 replica of the left ventricle and the 55 largest human conduit arteries made by Segers et al. (1998). A successful validation of our code against another numerical method has also been published (Sherwin et al., 2003a), along with an application to the study of monochorionic placentas (Franke et al., 2003).

Our objective is to investigate the effects of the most frequent anatomical variations and diameters of the CoW on cerebral outflows and pulse wave propagation, in

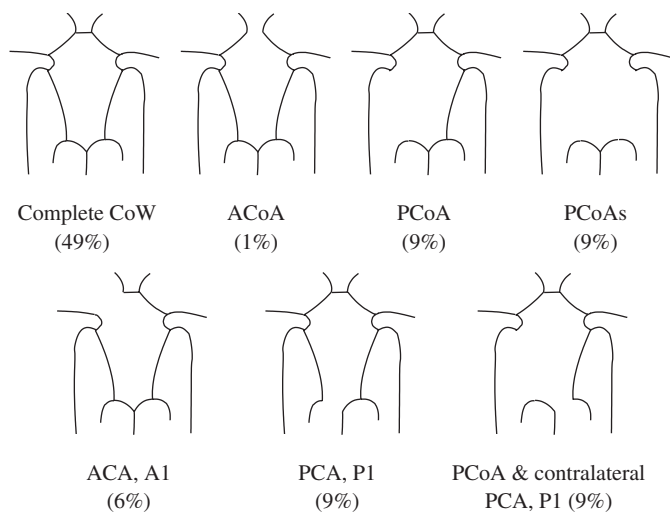


Fig. 2. Anatomical variations of the CoW studied. In each case, we indicate the artery absent (depicted only on one side, but it can also be absent on the other side) and its frequency, according to Lippert and Pabst (1985). We do not consider variations involving vessels outside the CoW.

healthy conditions and after a complete occlusion of an ICA or a VA. This study is limited to the most frequent anatomical variations reported in Lippert and Pabst (1985) with one or two circulus arteries absent or hypoplastic (simulated as absent). Fig. 2 shows the cases studied and their estimated frequency. Although the ACoA is missing in less than 1% of the cases, we include this anatomical variation because the ACoA is commonly recognised as the functionally most important collateral route in case of severe occlusion of an ICA (Cassot et al., 1995; Hillen et al., 1988; Hoksbergen et al., 2000b).

## 2. Methodology

### 2.1. Mathematical model

#### 2.1.1. Governing equations

The mathematical model is based on the non-linear, 1-D equations of pressure and flow wave propagation in compliant vessels. The governing system of equations results from conservation of mass and momentum applied to a 1-D impermeable and deformable tubular control volume of incompressible and Newtonian fluid. They take the form (Sherwin et al., 2003b; Alastruey, 2006)

$$\frac{\partial A}{\partial t} + \frac{\partial(AU)}{\partial x} = 0, \quad (1)$$

$$\frac{\partial U}{\partial t} + U \frac{\partial U}{\partial x} = -\frac{1}{\rho} \frac{\partial p}{\partial x} + \frac{f}{\rho A}, \quad (2)$$

where  $x$  is the axial coordinate along the vessel,  $t$  is the time,  $A(x, t)$  is the cross-sectional area of the vessel,  $U(x, t)$  is the average axial velocity,  $p(x, t)$  is the average internal pressure over the cross-section,  $\rho$  is the density of the blood taken here to be  $1050 \text{ Kg m}^{-3}$  and  $f(x, t)$  is the friction force per unit length, which is modelled as  $f = -22\pi\mu U$  according to Smith et al. (2001), with  $\mu$  the viscosity of the blood taken here to be  $4.5 \text{ mPa s}$ .

The system of equations is completed with a pressure–area relation previously used in Olufsen (1999), Sherwin et al. (2003b), Alastruey (2006). It assumes a thin, homogeneous and elastic arterial wall and it takes the form

$$p = p_0 + \frac{\beta}{A_0} (\sqrt{A} - \sqrt{A_0}), \quad \beta = \frac{\sqrt{\pi} h E}{(1 - \sigma^2)}, \quad (3)$$

where  $A_0$  and  $h$  are the sectional area and wall thickness at the reference state ( $p_0, U_0$ ), with  $p_0$  and  $U_0$  assumed to be zero,  $E$  is the Young's modulus and  $\sigma$  is the Poisson's ratio, typically taken to be  $\sigma = \frac{1}{2}$  since biological tissue is practically incompressible. The parameter  $\beta$  is related to the speed of pulse wave propagation,  $c$ , through (Sherwin et al., 2003b; Alastruey, 2006)

$$c^2 = \frac{\beta}{2\rho A_0} A^{1/2}. \quad (4)$$

**2.1.2. Treatment of boundary conditions and bifurcations**

The hyperbolic system of partial differential equations (1)–(3) is solved in each arterial segment of Fig. 1 (right) with the following boundary conditions. At the proximal end of the ascending aorta we enforce a periodical inflow rate  $Q(t)$  with a period of 1 s. Each period consists of a half-sinusoidal flow rate wave with a peak value  $\hat{Q}$  of  $485 \text{ ml s}^{-1}$  (adjusted to produce a physiological cardiac output and aortic mean pressure with the peripheral resistances shown in Table 1) and a duration  $\tau = 0.3 \text{ s}$  (systole). Flow rate is zero in the rest of the period (diastole),

$$Q(t) = \begin{cases} \hat{Q} \sin\left(\frac{\pi t}{\tau}\right) & \text{if } t < \tau, \\ 0 & \text{otherwise.} \end{cases} \quad (5)$$

This boundary condition acts as a total reflector when flow rate is zero, simulating the closure of the aortic valve during diastole.

Boundary conditions of the arterial segments joining at junctions are prescribed by enforcing conservation of mass

and continuity of the total pressure  $p + \frac{1}{2}\rho U^2$ . The distal end of each terminal branch is coupled to a three-element lumped parameter model, consisting of two resistances,  $R_1$  and  $R_2$ , and a compliance,  $C$ , to account for both the resistive and the compliant effects of the vessels supplied by the terminal arteries. This terminal model produces more physiological pulse waves than a purely reflective model, as used in Sherwin et al. (2003b); Wang and Parker (2004), because it partially reflects and smoothes any incoming wave, causing a phase delay between pressure and flow. It is governed by the differential equation

$$p_{1D} + R_2 C \frac{dp_{1D}}{dt} = p_v + (R_1 + R_2)Q_{1D} + R_1 R_2 C \frac{dQ_{1D}}{dt}, \quad (6)$$

where  $p_{1D}$  and  $Q_{1D}$  are the pressure and volume flow rate at the distal end of the 1-D terminal artery, and  $p_v$  represents the pressure at the entrance of the venous system, taken to be 5 mmHg.

Table 1

Physiological data used in the model shown in Fig. 1 (right) based upon the data collected by Stergiopoulos et al. (1992), Fahrig et al. (1999) and Moore et al. (2006)

| Arterial segment       | Length (cm) | Initial radius (cm) | Thickness (cm) | Elastic modulus ( $10^6 \text{ Pa}$ ) | Peripheral resistance ( $10^9 \text{ Pa s m}^{-3}$ ) | Peripheral compliance ( $10^{-10} \text{ m}^3 \text{ Pa}^{-1}$ ) |
|------------------------|-------------|---------------------|----------------|---------------------------------------|--|--|
| 1. Ascending aorta     | 4.0         | 1.200               | 0.163          | 0.4                                   | —  | —  |
| 2. Aortic arch I       | 2.0         | 1.120               | 0.126          | 0.4                                   | —  | —  |
| 3. Brachiocephalic     | 3.4         | 0.620               | 0.080          | 0.4                                   | —  | —  |
| 4. Aortic arch II      | 3.9         | 1.070               | 0.115          | 0.4                                   | —  | —  |
| 5. L. common carotid   | 20.8        | 0.250               | 0.063          | 0.4                                   | —  | —  |
| 6. R. common carotid   | 17.7        | 0.250               | 0.063          | 0.4                                   | —  | —  |
| 7. R. subclavian       | 3.4         | 0.423               | 0.067          | 0.4                                   | —  | —  |
| 8. Thoracic aorta      | 15.6        | 0.999               | 0.110          | 0.4                                   | 0.18   | 38.70  |
| 9. L. subclavian       | 3.4         | 0.423               | 0.067          | 0.4                                   | —  | —  |
| 10. L. ext. carotid    | 17.7        | 0.150               | 0.038          | 0.8                                   | 5.43   | 1.27   |
| 11. L. int. carotid I  | 17.7        | 0.200               | 0.050          | 0.8                                   | —  | —  |
| 12. R. int. carotid I  | 17.7        | 0.200               | 0.050          | 0.8                                   | —  | —  |
| 13. R. ext. carotid    | 17.7        | 0.150               | 0.038          | 0.8                                   | 5.43   | 1.27   |
| 14. R. vertebral       | 14.8        | 0.136               | 0.034          | 0.8                                   | —  | —  |
| 15. R. brachial        | 42.2        | 0.403               | 0.067          | 0.4                                   | 2.68   | 2.58   |
| 16. L. brachial        | 42.2        | 0.403               | 0.067          | 0.4                                   | 2.68   | 2.58   |
| 17. L. vertebral       | 14.8        | 0.136               | 0.034          | 0.8                                   | —  | —  |
| 18. L. int. carotid II | 0.5         | 0.200               | 0.050          | 1.6                                   | —  | —  |
| 19. L. PCoA            | 1.5         | 0.073               | 0.018          | 1.6                                   | —  | —  |
| 20. R. PCoA            | 1.5         | 0.073               | 0.018          | 1.6                                   | —  | —  |
| 21. R. int. carotid II | 0.5         | 0.200               | 0.050          | 1.6                                   | —  | —  |
| 22. Basilar            | 2.9         | 0.162               | 0.040          | 1.6                                   | —  | —  |
| 23. L. MCA             | 11.9        | 0.143               | 0.036          | 1.6                                   | 5.97   | 1.16   |
| 24. R. MCA             | 11.9        | 0.143               | 0.036          | 1.6                                   | 5.97   | 1.16   |
| 25. L. ACA, A1         | 1.2         | 0.117               | 0.029          | 1.6                                   | —  | —  |
| 26. R. ACA, A1         | 1.2         | 0.117               | 0.029          | 1.6                                   | —  | —  |
| 27. L. PCA, P1         | 0.5         | 0.107               | 0.027          | 1.6                                   | —  | —  |
| 28. R. PCA, P1         | 0.5         | 0.107               | 0.027          | 1.6                                   | —  | —  |
| 29. L. ACA, A2         | 10.3        | 0.120               | 0.030          | 1.6                                   | 8.48   | 0.82   |
| 30. R. ACA, A2         | 10.3        | 0.120               | 0.030          | 1.6                                   | 8.48   | 0.82   |
| 31. ACoA               | 0.3         | 0.074               | 0.019          | 1.6                                   | —  | —  |
| 32. L. PCA, P2         | 8.6         | 0.105               | 0.026          | 1.6                                   | 11.08  | 0.62   |
| 33. R. PCA, P2         | 8.6         | 0.105               | 0.026          | 1.6                                   | 11.08  | 0.62   |

At any point in the network we can simulate a total occlusion by enforcing the condition  $U = 0$  at the desired point, or a partial occlusion by decreasing locally the calibre of the artery.

### 2.1.3. Numerical scheme

Eqs. (1)–(3) are solved using a discontinuous Galerkin scheme with a spectral/ $hp$  spatial discretisation and a second-order Adams–Bashforth time-integration scheme. This scheme is suitable for the 1-D formulation because it can propagate waves of different frequencies without suffering from excessive dispersion and diffusion errors. Details on this algorithm can be found in (Karniadakis and Sherwin, 2003; Sherwin et al., 2003b).

### 2.2. Physiological data

The physiological parameters used in each arterial segment are given in Table 1. Our model aims at representing the arterial geometry and elasticity of a healthy young adult. In the absence of detailed knowledge of these properties, the geometry and wall elasticity of the arteries up to the carotids and vertebrales are based on data published in Stergiopoulos et al. (1992). In the cerebral arteries, we consider the lengths published in Fahrig et al. (1999), obtained from average values from several published sources. The radii at the reference state ( $p_0, U_0$ ) correspond to an average of 13 magnetic-resonance angiographies (MRAs) of complete CoWs (Moore et al., 2006). In all the cerebral vessels, we assume  $h$  to be 25% of the radius at reference conditions. In the carotids and VAs we consider  $E = 8 \times 10^5$  Pa, and in the remaining vessels  $E = 16 \times 10^5$  Pa, since they are stiffer than extracranial arteries with similar calibres (Hayashi et al., 1980).

At the distal end of each terminal branch, we assume  $R_1$  to be equal to the characteristic impedance of the terminal branch,  $Z_0 = \rho c_0/A_0$  with  $c_0 = c(A_0)$  (4), since it is the value that minimises the total impedance of the three-element lumped parameter model (Rainest et al., 1974). The total resistance of the arterial system in normal conditions is considered to be  $R_T = 1.34 \times 10^8$  Pa s m<sup>-3</sup>, according to Stergiopoulos et al. (1992). The value of each peripheral resistance  $R_p = R_1 + R_2$  is determined by assuming the following flow distribution in normal conditions: 15% of the cardiac output perfuses the head (Burton, 1965), 5% supplies each arm and 75% flows to the rest of the body through the thoracic aorta. In the terminal vessels of the head, outflows are assumed to be proportional to the initial cross-sectional areas of the perfusing terminal arteries.

The total volume compliance of the arterial system in normal conditions is taken to be  $9.45 \times 10^{-9}$  m<sup>3</sup> Pa<sup>-1</sup> (Simon et al., 1979). This value corresponds to the compliance of each arterial segment, calculated through  $A_0 l / \rho c_0^2$  ( $l$  is the length of the segment) (Milišić and Quarteroni, 2004), plus the total peripheral compliance. In the absence of any data, we distribute the total peripheral

compliance among the terminal branches in the same proportion as the flow distribution determined by the peripheral resistances.

## 3. Results and discussion

Our algorithm allows us to easily modify the geometry and connectivity of each arterial segment, to partially or totally occlude arteries, and to calculate pressure and flow time histories at any point in the system. We initially assume  $A(x, 0) = A_0$  and  $U(x, 0) = 0$  in all the arteries, and we run each simulation for sufficient cardiac cycles until the waveforms become periodic. This typically takes around 10 cycles.

In Section 3.1, we analyse pressure and flow wave propagation along the aorta, the brachiocephalic bifurcation and the rest of vessels supplying the CoW. In Section 3.2, we investigate how cerebral flows are affected by anatomical variations (Section 3.2.1), by the total occlusion of an ICA or a VA (Section 3.2.2) and by several degrees of partial occlusions of the communicating arteries (Section 3.2.3). This study focuses on flow rates, because they are clinically important in brain perfusion and they can be measured non-invasively with phase-contrast MR (PC-MR) (Cebal et al., 2003), and on flow velocity patterns, which can be measured non-invasively with transcranial colour-coded duplex ultrasonography (TCCD) (Hoksbergen et al., 2003) and PC-MR (Cebal et al., 2003).

### 3.1. Wave propagation along the aorta and in the arteries supplying the CoW

Our model is able to capture the main wave propagation features observed in in vivo measurements along the aorta (McDonald, 1960; O'Rourke, 1967), such as the increase in pulse pressure as we move away from the heart, the diastolic notch at the end of systole and the diastolic decay due to the windkessel effect (Fig. 3, left). Moreover, the peak flow decreases as we move down the aorta, though the characteristic backward flow after the closure of the aortic valve is almost absent (Fig. 3, right), because of the approximated inflow rate (5) at the inlet of the ascending aorta without any reversal flow. At the inlet of the ascending aorta, the systolic pressure is 17.3 kPa (130 mmHg) and the diastolic pressure is 10.1 kPa (76 mmHg). The cardiac output is 5.7 l min<sup>-1</sup>.

Our model is also able to predict the in vivo observed pressure and flow patterns at the brachiocephalic bifurcation. In vivo Doppler measurements of velocity in the brachiocephalic artery (BrA) (parent) and the right SCA and CCA (daughters) of a healthy young adult (all taken approximately 1 cm from the bifurcation) show a significant difference between velocity waveforms (Fig. 4, top). Flow is always directed towards the head (antegrade) in the CCA, ensuring cerebral blood supply at any instant during the cardiac cycle, whereas in the BrA and right SCA flow is biphasic, with a period of backward flow at the end of

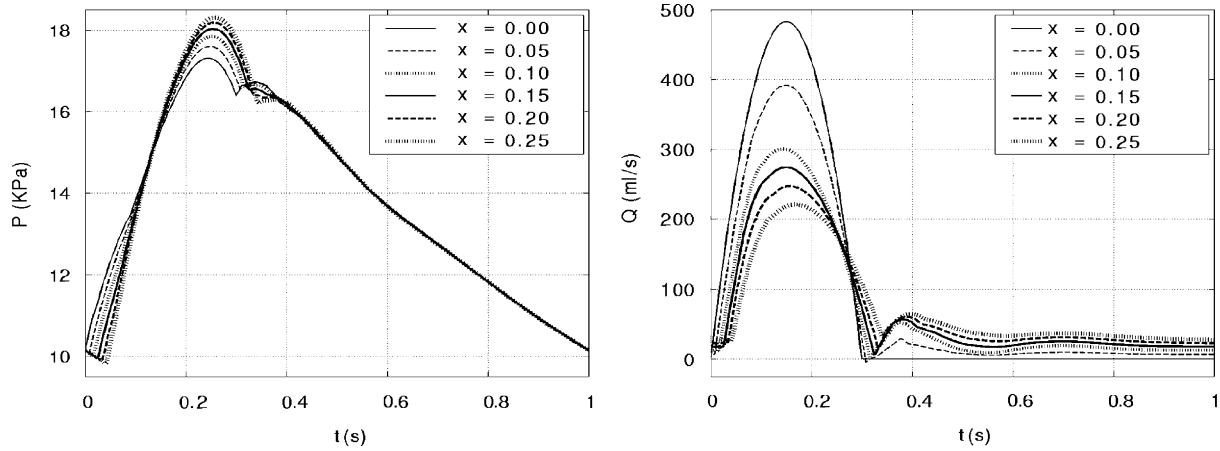


Fig. 3. Pressure (left) and flow volume rate (right) over one cardiac cycle along the aorta. The legend indicates the distance of the measurement from the left ventricle.

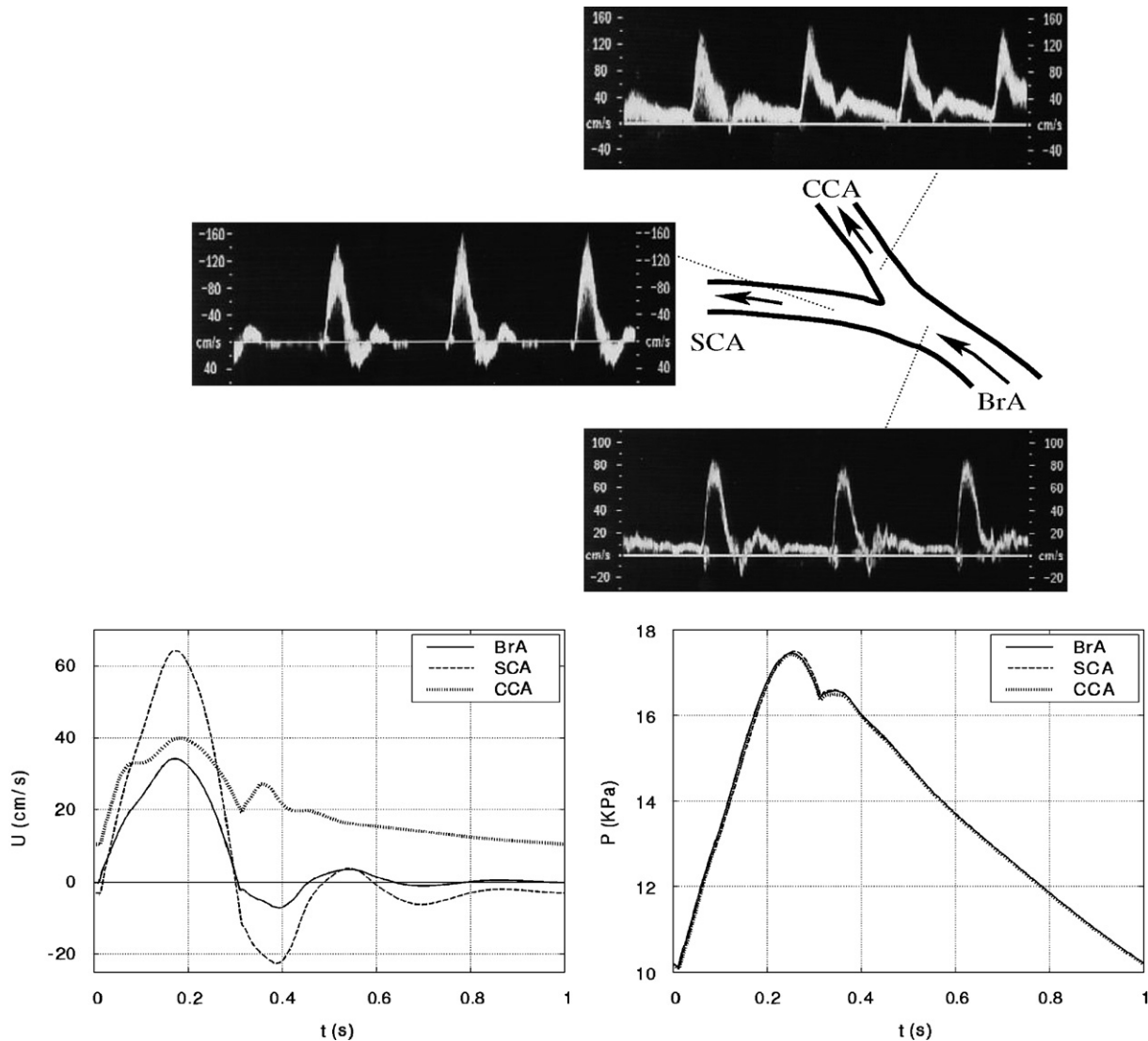


Fig. 4. Flow velocity at the brachiocephalic (BrA), right subclavian (SCA) and right common carotid (CCA) arteries measured in vivo with Doppler ultrasound in a healthy young adult (top) and predicted by our model 1 cm proximal to the bifurcating point (bottom left). We also show the predicted pressures (bottom right).

systole. These measurements are in agreement with the velocity waveforms from a young normal subject published by Oates (2001). The results predicted by our simulation in the BrA and the right SCA and CCA are in good qualitative agreement with the in vivo measurements (Fig. 4, bottom left). We notice that a quantitative comparison cannot be achieved because we lack information about the inflow at the ascending aorta, the arterial geometry and elasticity and the terminal impedances of our subject. The simulated flow patterns where the left CCA branches off the aortic arch and the two VAs branch off the corresponding SCA present the same pattern as in the brachiocephalic bifurcation, so that flow is always antegrade during the cardiac cycle in the four arteries perfusing the head. These results are also in agreement with the Doppler measurements published by Oates (2001).

According to our model, flow is antegrade in the CCAs and the VAs of all the anatomical variations depicted in Fig. 2, even though the predicted pressure waveforms in these vessels are very similar to the corresponding pressures in their adjacent arteries (Fig. 4, bottom right). Therefore, antegrade flow is a consequence of the length, diameter, elasticity and mean flow (determined by the terminal resistances) of the CCAs, VAs and their adjacent arteries.

### 3.2. Flow in the cerebral arteries

#### 3.2.1. Normal conditions

Our model predicts very similar flow patterns in all the efferent arteries of the complete CoW (Fig. 5, left), with flows always directed towards the brain. Differences between the same efferent artery at both sides of the CoW cannot be appreciated in the scale of the figure, which indicates that flows in the cerebral arteries are not affected by the asymmetry introduced by the BrA. Table 2 (first study case) shows the mean volume outflows in the cerebral

arteries. We observe that the MCAs receive the highest blood supply, followed by the ACAs. The values and distribution of these outflows are within acceptable physiological ranges compared to average in vivo measurements calculated in Fahrig et al. (1999) based on several published sources (last row of Table 2).

Fig. 5 (left) shows that flows in the communicating arteries are small but sufficiently significant to maintain these vessels active. They arise from pressure phase delays between both sides of the CoW, as a consequence of the asymmetry introduced by the BrA. Table 2 shows that the volume flow rates along these arteries are about two orders of magnitude smaller than the volume outflow rates in the efferent arteries, which suggests that the system does not require the collateral flow pathways through the communicating arteries to adequately perfuse the brain of healthy subjects with a complete CoW. Their MCAs and ACAs are supplied with flow coming mainly from the ipsilateral ICA and their PCAs with flow through the basilar artery.

Anatomical variations with missing communicating arteries present mean volume outflow rates in the efferent arteries and the remaining communicating arteries that differ in less than 1% the results obtained for the complete CoW (Table 2). The flow patterns in their efferent arteries also differ in less than 1% the results shown in Fig. 5 (left) for the complete CoW.

When one of the ACAs (A1) or PCAs (P1) is absent or hypoplastic, our model predicts high collateral volume flow rates through the communicating arteries, since they are the only possible pathway to an efferent vessel (Table 2). Flows in the efferent arteries present the same patterns as shown in Fig. 5 (left) for the complete CoW, though with differences of less than 15% in the value of flow velocities. In terms of mean volume outflows, the differences between these anatomies and a complete CoW are also less than 15% (Table 2), which suggests that collateral flows through

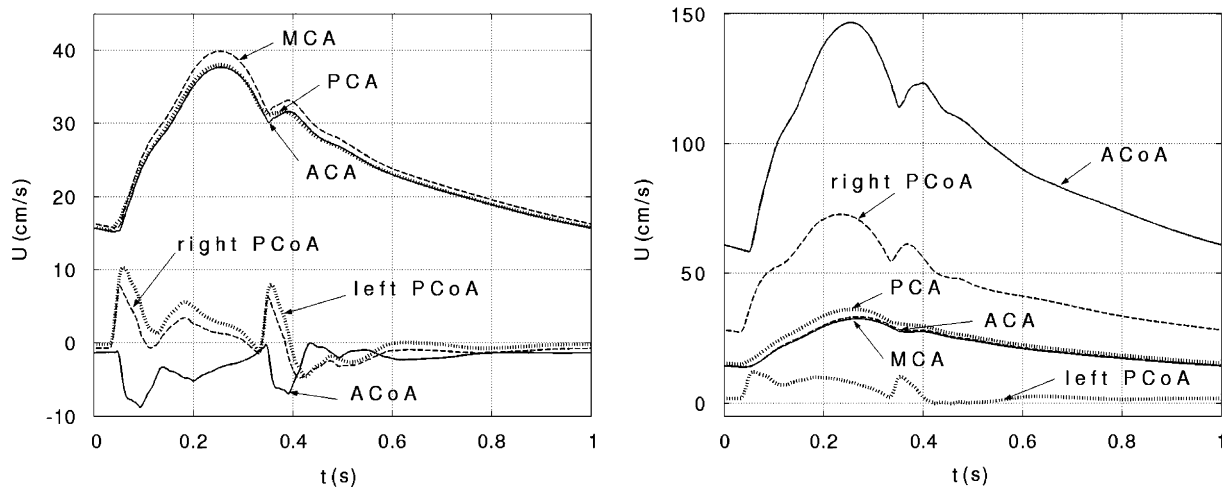


Fig. 5. Flow velocity over one cardiac cycle in the middle point of the efferent and communicating arteries of the complete CoW, in normal conditions (left) and after occlusion of the right ICA (right). In normal conditions, the results in the same cerebral vessel at both sides of the CoW cannot be distinguished in the scale of the figure. With the occlusion, only the results on the right side are shown. On the left side, they present a similar pattern but with slightly higher values. Positive values in the communicating arteries follow the direction of the arrows in Fig. 1 (right).

Table 2

Mean volume flow rates (in ml/s) at the outlet of the efferent arteries and in the middle of the communicating arteries for different study cases

| Study case                 | RACA | LACA | RMCA | LMCA | RPCA | LPCA | RPCoA | LPCoA | ACoA  |
|----------------------------|------|------|------|------|------|------|-------|-------|-------|
| Complete circle            | 1.16 | 1.16 | 1.73 | 1.72 | 0.90 | 0.89 | −0.01 | 0.01  | −0.05 |
| ACoA absent                | 1.16 | 1.16 | 1.73 | 1.72 | 0.90 | 0.89 | −0.01 | 0.02  | —     |
| RPCoA absent               | 1.16 | 1.16 | 1.73 | 1.72 | 0.89 | 0.89 | —     | 0.01  | −0.05 |
| LPCoA absent               | 1.16 | 1.16 | 1.73 | 1.72 | 0.90 | 0.90 | 0.00  | —     | −0.05 |
| PCoAs absent               | 1.16 | 1.16 | 1.73 | 1.72 | 0.90 | 0.90 | —     | —     | −0.05 |
| RACA (A1) absent           | 1.07 | 1.11 | 1.78 | 1.68 | 0.90 | 0.90 | −0.22 | 0.22  | 1.07  |
| LACA (A1) absent           | 1.12 | 1.08 | 1.69 | 1.78 | 0.90 | 0.90 | 0.18  | −0.19 | −1.08 |
| RPCA (P1) absent           | 1.15 | 1.16 | 1.70 | 1.72 | 0.79 | 0.93 | −0.79 | 0.27  | 0.21  |
| LPCA (P1) absent           | 1.16 | 1.15 | 1.73 | 1.70 | 0.93 | 0.79 | 0.25  | −0.79 | −0.32 |
| RPCA (P1) and LPCoA absent | 1.15 | 1.15 | 1.70 | 1.71 | 0.79 | 0.94 | −0.79 | —     | 0.14  |
| LPCA (P1) and RPCoA absent | 1.15 | 1.14 | 1.72 | 1.69 | 0.94 | 0.79 | —     | −0.79 | −0.25 |
| Fahrig et al. (1999)       | 1.1  | 1.1  | 2.0  | 2.0  | 0.8  | 0.8  | —     | —     | —     |

The last row shows an average of published in vivo measurements at the efferent arteries calculated by Fahrig et al. (1999). Positive values of flow in the communicating arteries follow the direction of the arrows in Fig. 1 (right). R stands for right and L for left.

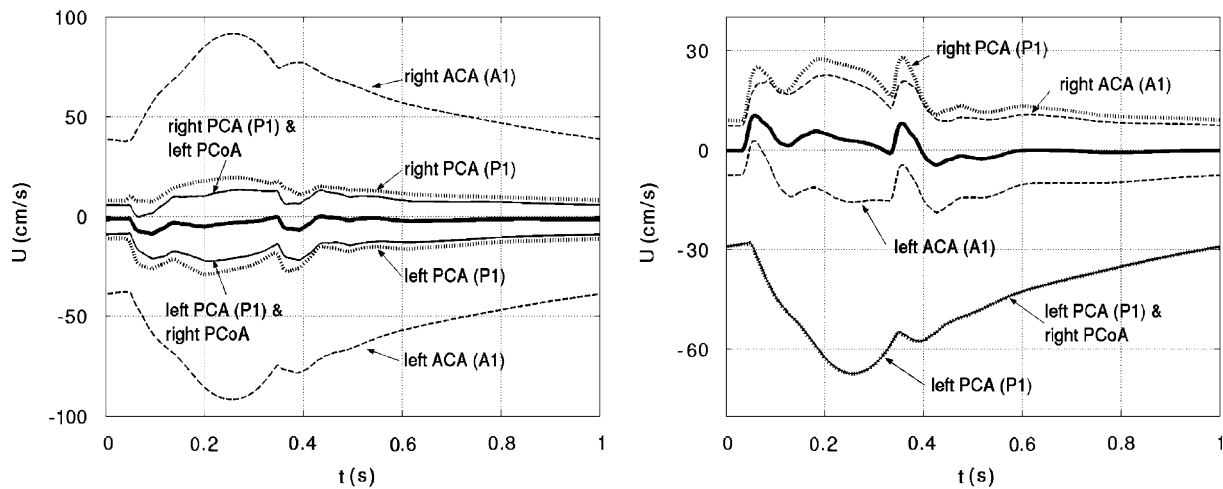


Fig. 6. Flow velocity over one cardiac cycle in the middle point of the ACoA (left) and the left PCoA (right) (similar results are obtained in the right PCoA) of the complete CoW (thick solid lines) and the anatomical variations with missing vessels as indicated in the figures. Positive values follow the direction of the arrows in Fig. 1 (right). We notice that the direction of flow in the ACoA and the PCoAs depends upon the side of the CoW where there is the hypoplastic ACA (A1) or PCA (P1).

the communicating arteries are sufficient to perfuse all the areas of the brain in subjects with a hypoplastic ACA (A1) or PCA (P1). Although fluxes are reduced in some efferent vessels, the vasoconstriction and vasodilatation of the cerebral vessels and the wall remodelling in the active collateral vessels to increase the calibre of their lumen are likely to compensate for any reduction in blood flows. However, these autoregulation mechanisms have not been considered in our simulations.

Therefore, when flow or volume flow rate in any communicating artery is high enough to be measured in a patient without a significant stenosis in any afferent artery, at least one of the ACAs (A1) or PCAs (P1) is hypoplastic. Fig. 6 (left) shows that the direction of flow in the ACoA indicates the side of the CoW where there is a hypoplastic ACA (A1) or PCA (P1). Furthermore, flow waveforms in the ACoA are similar to flow waveforms in the ACAs (A2) in anatomies with a hypoplastic ACA (A1), which suggests that TCCD measurements in the ACoA should allow us to

detect the presence of a dysfunctional ACA (A1). The direction of flow in the PCoAs also indicates the side where there is a dysfunctional ACA (A1) or PCA (P1) (Fig. 6, right). In this case, flow waveforms in a PCoA are similar to flow waveforms in the ipsilateral PCA (P2) if the ipsilateral PCA (P1) is hypoplastic.

The mean flow rates given in Table 2 depend on the input flow rate enforced at the ascending aorta and the peripheral resistances. For the cases with an absent ACA (A1) or PCA (P1) they also depend on the resistance of the communicating arteries. Consequently, cerebral mean flow rates are very sensitive to changes in the geometry and elasticity of the communicating arteries when an ACA (A1) or PCA (P1) is absent. Changes in the rest of the arteries simulated (within physiological ranges) affect pulse waveforms but not mean flows.

Finally, we notice that MRA techniques may not be able to detect the presence of the communicating arteries in subjects with a complete CoW or with anatomical

variations involving these arteries, since flow velocities in the communicating arteries of these anatomies are about two orders of magnitude smaller than in the rest of the cerebral vessels, according to our model.

3.2.2. The effects of occlusions of the afferent arteries

The occlusion of an ICA considerably increases flow in the communicating arteries of the complete CoW (Fig. 5, right) and all the anatomical variations studied.

Fig. 7 shows the ability of each anatomical variation in Fig. 2 to maintain sufficient efferent outflow rates after an occlusion of either the right ICA (dark numbers) or the right VA (light numbers). The number at the outlet of each efferent artery indicates the percentage of reduction in mean outflow rate calculated as  $(Q_{NC} - Q_{OC})/Q_{NC} \times 100$ , where  $Q_{NC}$  is the mean outflow rate in normal conditions (shown in Table 2) and  $Q_{OC}$  is the mean outflow rate with the occlusion.

We notice that in all the cases studied the occlusion of the VA has relative little effect compared to the occlusion of the ICA. If the right ICA is occluded, the right MCA is the efferent artery with the highest reduction in outflow rate in all the anatomies, followed by the right ACA (A2). In anatomical variations involving the communicating arteries, the absence of the ACoA is the case with the highest decrease in efferent mean outflows, because collateral flow from the left ICA to the right ACA (A2) and MCA has less viscous dissipation through the ACoA than through the PCoAs, since the former route is shorter. Hence, the ACoA is a more critical collateral pathway than both PCoAs if an ICA is occluded. This is in agreement with the results obtained in Cassot et al. (1995), Hillen et al. (1988), Hoksbergen et al. (2000b). If the right VA is occluded, the PCAs (P2) are the efferent arteries with the highest reduction in flow rates and the PCoAs become the

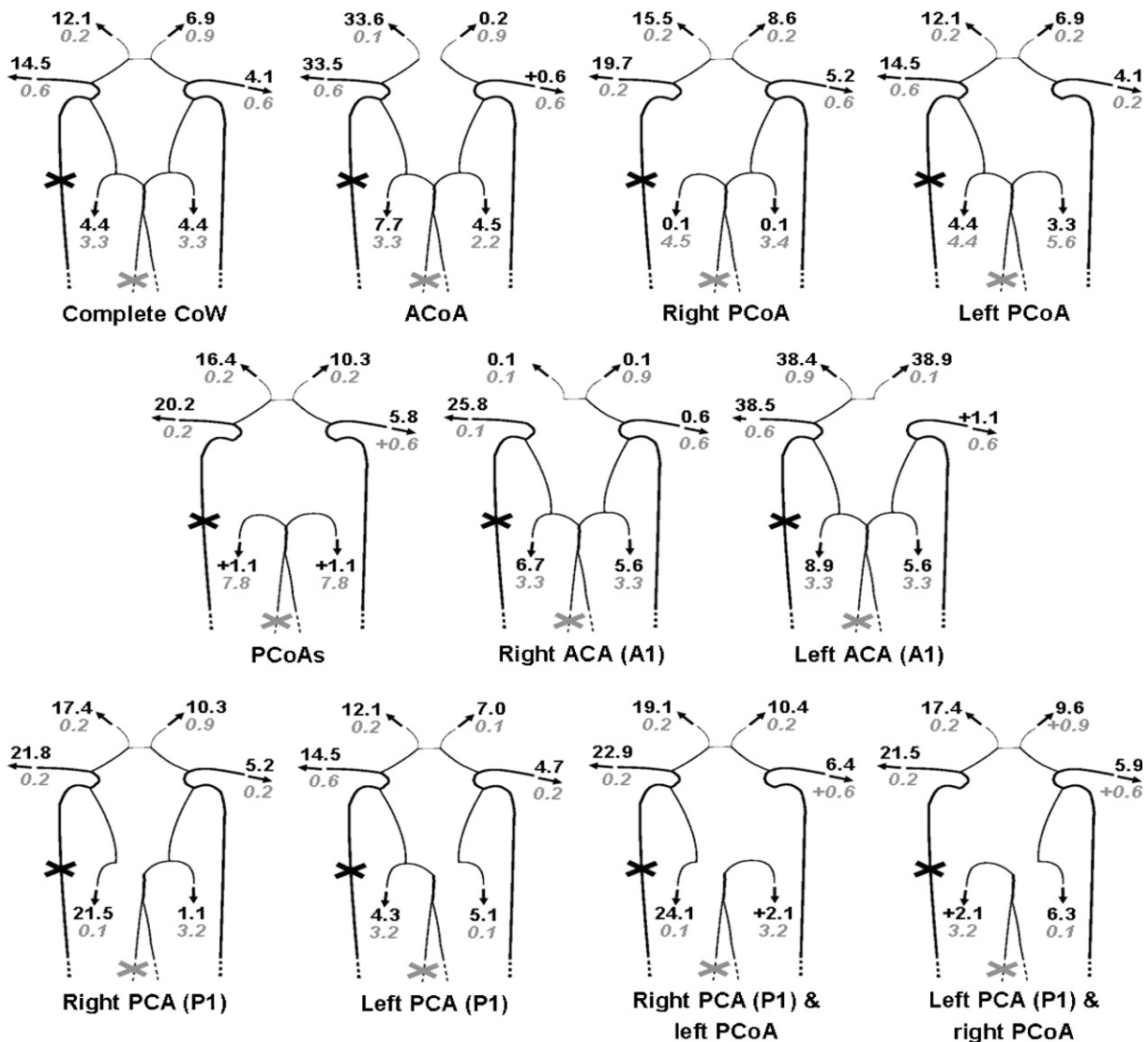


Fig. 7. Reduction in mean outflow rate at the outlet of the efferent arteries of each anatomical variation studied (the arteries absent are indicated at the bottom of each case), when the right ICA (black numbers) or the right VA (light numbers) are occluded. Numbers express the percentage of reduction in mean outflow rate with the occlusion, as explained in the text. Numbers with “+” indicate an increase in mean outflow rates.

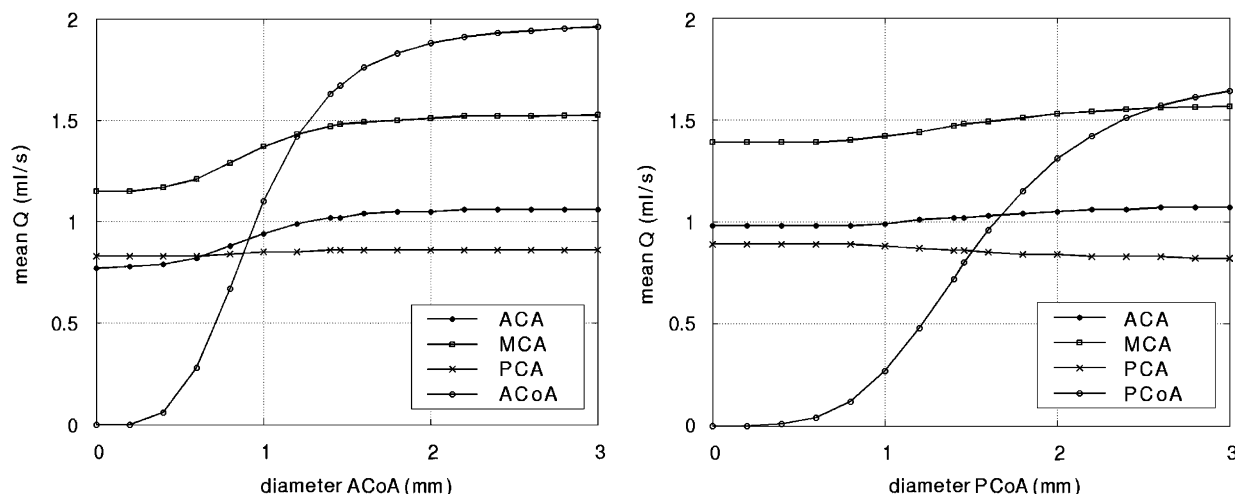


Fig. 8. Mean outflows in the right efferent arteries and in the ACoA and right PCoA of the complete CoW as a function of the diameter of the ACoA (left) and the right PCoA (right). The right ICA is completely occluded in its middle point.

collateral routes that play a more important role in the compensatory mechanism of the CoW.

Among all the cases studied, the anatomical variation without an ACA (A1) and with a complete occlusion of the contralateral ICA presents the highest reduction in mean outflow rates in three efferent arteries. Therefore, we conclude that this is the anatomy at the highest risk of TIA and cerebral stroke.

### 3.2.3. Partial occlusions of the communicating arteries

In this section we study the effect on cerebral flows of partial occlusions of the communicating arteries of the complete CoW combined with the occlusion of the right ICA. Fig. 8 shows the effect of the calibre of the ACoA (left) and the right PCoA (right) on the mean outflow rates in the three right efferent arteries, when the right ICA is completely occluded in its middle point. We observe that the outflows of the ACA (A2) and the MCA depend strongly on the calibre of the ACoA in the range of calibres from 0.4 to 1.6 mm, approximately, whereas the outflow at the PCA (P2) remains almost constant in all the range of calibres studied. On the other hand, the calibre of the right PCoA affects the outflows at the three efferent arteries, specially in the range of calibres from 0.8 to 2.2 mm. For a given calibre, collateral flow through the ACoA is higher than through the right PCoA. Furthermore, a reduction in the calibre of the ACoA produces a higher reduction in the mean flow rates of the ACA (A2) and MCA than a reduction in the calibre of the right PCoA. These observations confirm the previous results showing that the ACoA is a more important collateral pathway than the PCoAs if an ICA is occluded.

We also observe that the mean flow rate of the right PCA (P2) decreases with increasing calibre of the right PCoA, since more blood from the posterior circulation is transported to the anterior circulation through the PCoA.

Using TCCD measurements and postmortem anatomy, Hoksbergen et al. (2000a) determined that the threshold diameter allowing for collateral flow through the communicating arteries is between 0.4 and 0.6 mm. Cassot et al. (1995) and Dickey et al. (1996) computationally obtained a threshold calibre of 0.4 mm for the ACoA. Moreover, Dickey et al. found that the threshold diameter for the PCoA in patients with a well-functioning ACoA and with an occlusion of an ICA is between 0.5 and 0.6 mm. According to our model, collateral flow in the ACoA starts for smaller calibres than in the PCoA (0.2 versus 0.4 mm). The efferent outflows significantly change for calibres higher than 0.4 mm in the ACoA and 0.8 in the PCoA, approximately (Fig. 8). We believe that the minimum diameter allowing for collateral flow through the PCoA is larger than through the ACoA because the longer length of the PCoAs compared to the length of the ACoA produces a higher resistance to flow.

## 4. Conclusions

We have presented a 1-D model of pulse wave propagation that is able to capture the main wave propagation features observed in vivo in the aorta, the cerebral arteries and the arteries supplying them from the aorta. From the origin of the carotid and VAs and up to the efferent vessels of the CoW, our model predicts a continuous blood flow towards the brain during all the cardiac cycles, which is in agreement with in vivo measurements (Fig. 4 and Oates, 2001).

We have used this model to study the effects of the most frequent anatomical variations of the CoW on flow rates and pulse waveforms in the communicating and efferent arteries. According to our results, the system does not require collateral pathways through the communicating arteries to adequately perfuse the brain of healthy subjects. The communicating arteries become important to maintain

sufficient brain perfusion in anatomical variations with a missing ACA (A1) or PCA (P1), or when an ICA or a VA is occluded. Moreover, the ACoA is a more critical collateral pathway than the PCoAs if an ICA is occluded, which is in agreement with other clinical and numerical studies (Cassot et al., 1995; Hillen et al., 1988; Hoksbergen et al., 2000b). If a VA is occluded, the reductions in mean efferent flow rates are significantly smaller than if an ICA is occluded, and the PCoAs are the collateral routes that play a more important role in the compensatory mechanism of the CoW. The worst scenario among all the anatomies studied in terms of reduction in the mean cerebral outflows is a CoW without an ACA (A1) and with a complete occlusion of the contralateral ICA.

Our model also predicts that in subjects without a significant stenosis in any afferent artery a hypoplastic ACA (A1) can be detected with flow measurements at the ACoA and a hypoplastic PCA (P1) with flow measurements at the PCoAs. Moreover, the direction of flow in the communicating arteries indicates the side of the CoW with such a hypoplastic artery. It is also important to notice that in subjects with a complete CoW or with anatomical variations involving the communicating arteries, flow velocities within these arteries may be too small for MRA techniques to detect their presence.

An obvious drawback of this study is the lack of experimental confirmation, because of the lack of detailed information on the geometry and elasticity of the arterial network and on the boundary conditions. The results presented depend on the physiological data used, which is based on published measurements in healthy young adults.

All the simulations have always been carried out with the same peripheral impedances and, hence, this work has analysed the compensatory ability of the CoW itself to reduce the effects of pathological alterations. This is the first mechanism of autoregulation that takes place. Other mechanisms such as vasodilatation, vasoconstriction and wall remodelling have been ignored. As mentioned previously, autoregulation by vasodilatation and vasoconstriction can be simulated with time-varying resistances (Ferrandez et al., 2002; David et al., 2003; Moorhead et al., 2004).

Our 1-D model is a fast and powerful research tool to enhance the understanding of blood flow patterns and distributions throughout the brain within a prescribed geometry. If used in conjunction with patient-specific geometry, it can predict the haemodynamic effect of clinical interventions such as carotid endarterectomy, angioplasty and stenting. It can be also applied to study the effect on cerebral outflows of time-dependent changes within the cardiac output, since it allows for a non-periodic inflow boundary condition at the ascending aorta. Furthermore, it has the potential to simulate local flows in detail if coupled to a 3-D simulation of a local area of the cerebral circulation, which, in turn, can be used to investigate, for instance, the flow patterns that lead to increased probability of formation of atherosclerosis or intracranial aneurysms.

## Acknowledgements

The authors would like to acknowledge Jazmín Aguado for her contributions. This work was partially supported by the EU RTN Haemodel Project (contract number HPRN-CT-2002-00270). The last author would also like to acknowledge partial support under an EPSRC Advanced Research Fellowship.

## References

- Alastruey, J., 2006. Numerical modelling of pulse wave propagation in the cardiovascular system: development, validation and clinical applications. Ph.D. Thesis, Departments of Bioengineering and Aeronautics, Imperial College London.
- Burton, A.C., 1965. Physiology and Biophysics of the Circulation. Year Book Medical Publishers.
- Cassot, F., Vergeur, V., Bossuet, P., Hillen, B., Zagzoule, M., Marc-Vergnes, J.P., 1995. Effects of anterior communicating artery diameter on cerebral hemodynamics in internal carotid artery disease. *Circulation* 92, 3122–3131.
- Cassot, F., Zagzoule, M., Marc-Vergnes, J.P., 2000. Hemodynamic role of the circle of Willis in stenoses of internal carotid arteries. An analytical solution of a linear model. *Journal of Biomechanics* 33, 395–405.
- Cebral, J.R., Castro, M.A., Soto, O., Löhner, R., Alperin, N., 2003. Blood-flow models of the circle of Willis from magnetic resonance data. *Journal of Engineering Mathematics* 47, 369–386.
- David, T., Brown, M., Ferrandez, A., 2003. Auto-regulation and blood flow in the cerebral circulation. *International Journal for Numerical Methods in Fluids* 43, 701–713.
- Dickey, P.S., Kailasath, P., Bloomgarden, G., Goodrich, I., Chaloupa, J., 1996. Computer modeling of cerebral blood flow following internal carotid occlusion. *Neurological Research* 18, 259–266.
- Fahrig, R., Nikolov, H., Fox, A.J., Holdsworth, D.W., 1999. A three-dimensional cerebrovascular flow phantom. *Medical Physics* 26, 1589–1599.
- Ferrandez, A., David, T., Brown, M., 2002. Numerical models of auto-regulation and blood flow in the cerebral circulation. *Computer Methods in Biomechanics and Biomedical Engineering* 5, 7–20.
- Franke, V.E., Parker, K.H., Wee, L.Y., Fisk, N.M., Sherwin, S.J., 2003. Time domain computational modelling of 1D arterial networks in monochorionic placentas. *Mathematical Modelling and Numerical Analysis* 37, 557–580.
- Hayashi, K., Handa, H., Nagasawa, S., Okumura, A., Moritake, K., 1980. Stiffness and elastic behavior of human intracranial and extracranial arteries. *Journal of Biomechanics* 13, 175–184.
- Henderson, R.D., Eliasziw, M., Fox, A.J., Rothwell, P.M., Barnett, H.J.M., 2000. Angiographically defined collateral circulation and risk of stroke in patients with severe carotid artery stenosis. *Stroke* 31, 128–132.
- Hillen, B., Hoogstraten, H., Post, L., 1986. A mathematical model of the flow in the circle of Willis. *Journal of Biomechanics* 19, 187–194.
- Hillen, B., Drinkenburg, A.H., Hoogstraten, H.W., Post, L., 1988. Analysis of flow and vascular resistance in a model of the circle of Willis. *Journal of Biomechanics* 21, 807–814.
- Hoksbergen, A.W.J., Fülesdi, B., Legemate, D.A., Csiba, L., 2000a. Collateral configuration of the circle of Willis. Transcranial color-coded duplex ultrasonography and comparison with postmortem anatomy. *Stroke* 31, 1346–1351.
- Hoksbergen, A.W.J., Legemate, D.A., Ubbink, D.T., Jacobs, M.J.H.M., 2000b. Collateral variations in circle of Willis in atherosclerotic population assessed by means of transcranial color-coded duplex ultrasonography. *Stroke* 31, 1656–1660.
- Hoksbergen, A.W.J., Majoie, C.B.L., Hulsmans, F.J.H., Legemate, D.A., 2003. Assessment of the collateral function of the circle of Willis: three-dimensional time-of-flight MR angiography compared with

- transcranial color-coded duplex sonography. *American Journal of Neuroradiology* 24, 456–462.
- Karniadakis, G.E., Sherwin, S.J., 2003. *Spectral/hp Element Methods for CFD*. Oxford University Press, Oxford.
- Lippert, H., Pabst, R., 1985. *Arterial Variations in Man: Classification and Frequency*. J.F. Bergmann, Munich.
- McDonald, D.A., 1960. *Blood Flow in Arteries*. Williams and Wilkins, Baltimore.
- Milišić, V., Quarteroni, A., 2004. Analysis of lumped parameter models for blood flow simulations and their relation with 1D models. *Mathematical Modelling and Numerical Analysis* 38, 613–632.
- Moore, S.M., Moorhead, K.T., Chase, J.G., David, T., Fink, J., 2005. One-dimensional and three-dimensional models of cerebrovascular flow. *Journal of Biomechanical Engineering* 127, 440–449.
- Moore, S.M., David, T., Chase, J.G., Arnold, J., Fink, J., 2006. 3D models of blood flow in the cerebral vasculature. *Journal of Biomechanics* 39, 1454–1463.
- Moorhead, K.T., Doran, C.V., Chase, J.G., David, T., 2004. Lumped parameter and feedback control models of the auto-regulatory response in the circle of Willis. *Computer Methods in Biomechanics and Biomedical Engineering* 7, 121–130.
- Oates, C., 2001. *Cardiovascular Haemodynamics and Doppler Waveforms Explained*. Greenwich Medical Media LTD.
- Olufsen, M.S., 1999. Structured tree outflow condition for blood flow in larger systemic arteries. *American Journal of Physiology* 276, H257–H268.
- O'Rourke, M.F., 1967. Pressure and flow waves in systemic arteries and the anatomical design of the arterial system. *Journal of Applied Physiology* 23, 139–149.
- Oshima, M., 2004. A new approach to cerebral hemodynamics. Patient-specific modelling and numerical simulation of blood and arterial wall interaction. *IACM Expressions* 16, 4–9.
- Rainest, J.K., Jaffrin, M.Y., Shapiro, A.H., 1974. A computer simulation of arterial dynamics in the human leg. *Journal of Biomechanics* 7, 77–91.
- Segers, P., Dubois, F., DeWachter, D., Verdonck, P., 1998. Role and relevancy of a cardiovascular simulator. *Cardiovascular Engineering* 3, 48–56.
- Sherwin, S.J., Formaggia, L., Peiró, J., Franke, V., 2003a. Computational modelling of 1D blood flow with variable mechanical properties and its application to the simulation of wave propagation in the human arterial system. *International Journal for Numerical Methods in Fluids* 43, 673–700.
- Sherwin, S.J., Franke, V., Peiró, J., Parker, K.H., 2003b. One-dimensional modelling of a vascular network in space–time variables. *Journal of Engineering Mathematics* 47, 217–250.
- Simon, A.C., Safar, M.E., Levenson, J.A., London, G.M., Levy, B.I., Chau, N.P., 1979. An evaluation of large arteries compliance in man. *American Journal of Physiology* 237, H550–H554.
- Smith, N.P., Pullan, A.J., Hunter, P.J., 2001. An anatomically based model of transient coronary blood flow in the heart. *SIAM Journal on Applied Mathematics* 62, 990–1018.
- Stergiopoulos, N., Young, D.F., Rogge, T.R., 1992. Computer simulation of arterial flow with applications to arterial and aortic stenoses. *Journal of Biomechanics* 25, 1477–1488.
- Viedma, A., Jiménez, C., Marco, V., 1997. Extended Willis circle model to explain clinical observations in periorbital arterial flow. *Journal of Biomechanics* 30, 265–272.
- Wang, J.J., Parker, K.H., 2004. Wave propagation in a model of the arterial circulation. *Journal of Biomechanics* 37, 457–470.